Inline Cavity Stepped Window Bandpass Filter With Two Transmission Zeros

Xuzhou Yu, *Student Member, IEEE*, Sai-Wai Wong, *Senior Member, IEEE*, Jing-Yu Lin, *Member, IEEE*, Yejun He, *Senior Member, IEEE*, Wenting Li, *Member, IEEE*, Long Zhang, *Member, IEEE*, Lei Zhu, *Fellow, IEEE*, and Li Yu

***Abstract*— This article proposed the design of bandpass filter (BPF) based on stepped window resonators (SWRs), which allows inline resonators to produce transmission zero (TZ). Compared with traditional cavity resonator using iris-coupled structure, the proposed SWR consists of two metal cavities, the larger cavity is regarded as a bandstop resonator to provide TZ near the passband. Therefore, each SWR pair can generate a transmission pole (TP) and a TZ. Two cavities are directly cascaded without any coupling iris, which increases the interface window between these two metal cavities and reduces the fabrication tolerance. By properly dimensioning the bandstop cavity, TZs can be generated in the lower and upper stopbands to improve the frequency-selective performance. An equivalent circuit model of SWR is proposed to explain the generation of TZ and synthesize the BPF. Finally, a fourth-order inline BPF with a fractional bandwidth of 1% at 10 GHz is designed using this SWR approach. The synthesis response and simulation results match well. The proposed BPF is fabricated and measured, and the good agreement between the measured and simulated results verifies the proposed design methodology.**

***Index Terms*— Equivalent circuit model, inline topology, stepped window resonator (SWR), transmission zeros (TZs).**

I. Introduction

MICROWAVE bandpass filters (BPFs) are widely used in microwave communication systems. Microstrip BPFs are very popular due to its planar structure [1], [2]. However, compared with waveguide resonators, insertion loss (IL) and power capacity of microstrip BPFs are not competitive. Due to the high quality factor and low IL, waveguide cavity filters are commonly designed and used in base station and satellite communication systems. Traditional cavity filters are designed by cavity resonators [3], [4], [5], [6], [7], [8], [9], [10], [11], [12], [13], [14], [15], [16], [17], [18], coaxial resonators [19], [20], and dielectric resonators [21], [22]. Iris/window resonators are rarely investigated to design microwave cavity filters [23], [24], [25], [26], [27], [28], [29], [30], [31], [32], [33], [34], [35]. Our previous works [23], [24] use iris resonators to improve the frequency selectivity and get wider bandwidth for both filter and antenna. A slot filtenna using iris resonators is proposed in [23], and it increases bandwidth by 20% without significantly increasing the circuit size. In [24], a cavity filtering crossover is presented, and the structure excites the resonance modes in cavities and the iris resonators simultaneously. The iris resonator contributes a wider fractional bandwidth (24%) and a compact size as the iris resonator provides additional resonant mode without adding extra circuit size. In [25], [26], [27], [28], and [29], some waveguide BPFs based on resonant irises have been presented, but the frequency selective performance is not very good since there is no transmission zero (TZ) in the frequency response. In addition, the design formula in [25] is an empirical equation, which is only 50% accuracy. A high-pass filter with three TZs at lower stopband is presented in [30], and the filter uses both cavities and irises as resonators simultaneously to make the passband wider. Two third-order BPFs with a TZ are presented in [31] and [32], and three transmission poles (TPs) consist of two cavity resonators and an iris resonator. Additionally, the TZ in [31] is attributed to higher order modes, which are excited in two cavities, while the TZ in [32] is provided by the crossing coupling through the iris. Recently, some inline quasi-elliptic BPFs [33], which use the iris resonators, are designed. It is noted that there are some TZs in the filters with inline topology, which improves the frequency selective performance. Moreover, two of these filters are fabricated by metal 3-D printing technology, which is easy to manufacture and reduces the cost of manufacturing. Three dual-band filters are presented in [34], and cavity and iris resonators are used to get two passbands, respectively. Moreover, the capacitive stubs are utilized to obtain TZs between the two passbands. Finally, the filter is cascaded with staircase configuration to suppress the first spurious passband. In [35], a wideband BPF with an inline structure is proposed by utilizing both cavity and iris resonators. The bandwidth is from 6.75 to 8.25 GHz because of the iris resonators, but the first spurious passband is from 9.5 GHz. Therefore, the filter is cascaded with the staircase configuration to suppress the first spurious passband,

Manuscript received 7 November 2022; revised 11 July 2023; accepted 11 July 2023. Date of publication 14 July 2023; date of current version 17 August 2023. This work was supported in part by the National Natural Science Foundation of China under Grant 62171289 and in part by the Shenzhen Science and Technology Programs under Grant JCYJ20190808145411289. Recommended for publication by Associate Editor W. T. Beyene upon evaluation of reviewers' comments. *(Corresponding authors: Sai-Wai Wong; Li Yu.)*

Xuzhou Yu, Sai-Wai Wong, Yejun He, Wenting Li, and Long Zhang are with the State Key Laboratory of Radio Frequency Heterogeneous Integration (Shenzhen University), College of Electronics and Information Engineering, Shenzhen University, Shenzhen 518060, China (e-mail: wongsaiwai@ieee.org).

Jing-Yu Lin is with the Institute of Electromagnetics and Acoustics, Xiamen University, Xiamen, Fujian 361005, China.

Lei Zhu is with the Department of Electrical and Computer Engineering, Faculty of Science and Technology, University of Macau, Macau, SAR, China.

Li Yu is with the Department of Computer Science, School of Basic Medicine Science, Tianjin Medical University, Tianjin 300071, China (e-mail: yuli@tmu.edu.cn).

Color versions of one or more figures in this article are available at https://doi.org/10.1109/TCPMT.2023.3295372.

Digital Object Identifier 10.1109/TCPMT.2023.3295372

which increases the volume of the filter. This filter is designed by WR-90, but it does not work in this frequency range, and it needs a waveguide transformer to convert the input to the desired frequency range, which increases the complexity and volume of the filter circuit.

The cavity filters with TZs are required in various communication systems. Traditionally, it is difficult to introduce a TZ in the inline topology, and novel coupling paths need to be introduced into the inline topology for generating TZs. Some papers [10], [11], [12], [13], [14] introduce some novel resonant elements in the inline topology or some novel coupling methods to create TZs. These works greatly contribute to the generation of TZs for inline topology structures. In [10], a novel coupling structure, which is a wire inside the cavity to realize the bypass coupling, is presented, and the structure enables bypass coupling without introducing additional cavities and enhances the frequency selectivity. In [11], a nonresonating mode waveguide filter is presented, and the filter consists of a cavity and two irises for coupling. TE_{201} mode is excited at the cavity and TE_{10} mode generates the source-load coupling to get a TZ. The filter in [11] is used to design two filters in [12] by cascading some filters in [11]. A stopband singlet is presented in [13], and the singlet consists of three cavities and two irises. There are two poles and a TZ, and the TE_{301} mode is excited at the coupled structure to generate source-load coupling. The structure is easy to fabricate. Therefore, the singlet can be used for designing waveguide filters. In [14], the singlet proposed in [13] is used to design a filter that has six poles and two TZs. It is worth noting that the paper [14] focuses on the synthesis design approach for waveguide cavity filters. The filter consists of two singlets in [14], and two cavities are an example of the synthesis design approach.

All the filters that use iris resonators are designed to make the passband wider, and none of them are narrowband filters with iris resonators. In this article, a stepped window BPF with two TZs is first presented. The fractional bandwidth is 1% at 10 GHz. The proposed BPF is fabricated by full metal cavities, and the stepped cavities produce four stepped window resonators (SWRs). Besides, the equivalent circuit models are created to explain the proposed SWR and BPF. Finally, compared with the inline cavity filters with TZs in [14] and [35], the volume of this proposed stepped window BPF is smaller.

II. SWR With TZ

This section demonstrates the study of the proposed SWR and its equivalent circuit model of the proposed resonator structure. Nonresonating discontinuity is a very common filter design method that has been applied to both microstrip filters and cavity filters. Therefore, the SWR filter proposed in this article may be misunderstood and considered to be the same structure as in [13]. What we would like to emphasize is that the stepped window filter proposed in this article resonates at the window region in between the large and small cavity, which uses the length of the rectangular waveguides that creates the SWR to adjust the coupling between two window resonators. In contrast, the traditional cavity filters

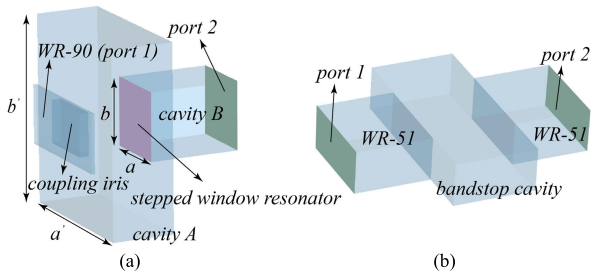

Fig. 1. Three-dimensional view. (a) Proposed SWR. (b) Bandstop singlet in [13].

use the cavity itself as a resonator and adjust the coupling strength through the size of iris, which is the most essential difference between the structure proposed in this article and the traditional filters.

Fig. 1(a) illustrates the 3-D view of the proposed SWR. Obviously, it is shown in Fig. 1(a) that the SWR consists of two different cavities (Cavities A and B), and the window (purple part) created by the discontinuity is a resonator. A standard waveguide (WR-90) is used as the input waveguide feeding port and an iris controls the coupling strength between the input and cavity A. Fig. 1(b) gives the 3-D view of the stopband singlet in [13], and it consists of two standard waveguides (WR-51) and a bandstop cavity. The structure in [13] uses a waveguide cavity as a resonator, and the input port is coupled to waveguide cavity through an iris. In order to prove that it is not resonating in the window and is different from our proposed SWR, the size of the coupling irises is enlarged to be the same as the waveguide, and the input and output ports are directly added to the WR-51. The designed SWR and the singlet in [13] are simulated in full-wave commercial software CST. Fig. 2(a) depicts the frequency response of the proposed SWR. Obviously, there is a TP at 10.05 GHz and a TZ at 9.20 GHz in Fig. 2(a), and the TP is created by the SWR. Besides, Fig. 2(b) gives the frequency response of the stopband singlet in Fig. 1(b). There is only a bandstop response at 20.16 GHz. Therefore, we can conclude that the singlet resonates at two cavities instead of the two windows in [13].

The two structures are simulated by eigenmode solver in CST. Fig. 3(a) and (b) shows the magnetic and electric field distributions of proposed SWR in two cavities. By looking at the field distribution, different modes in different cavities are excited. It can be seen from Fig. 3(a) and (b) that TM_{120} mode is excited in cavity A, while TE_{101} mode is excited in the adjacent cavity B. Fig. 3(c) and (d) depicts the surface current distribution of the proposed SWR and the bandstop singlet in [13]. It is obvious that the surface current distributions of the two structures are different, and the SWR resonates at the stepped window, while the bandstop singlet does not resonate at the window.

The high current density is caused by the presence of discontinuities in both E-plane and H-plane inside the cavity, which stores the electric and magnetic energy and produces parasitic inductance and parasitic capacitance around the stepped window structure [37]. With reference to [37], when an electromagnetic wave propagates in a rectangular waveguide, the magnetic field is compressed. When the electric and

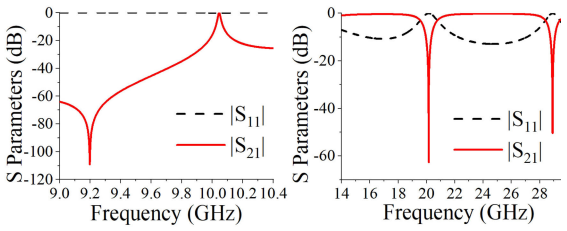

Fig. 2. Comparison of frequency responses. (a) Proposed SWR. (b) Bandstop singlet in [13].

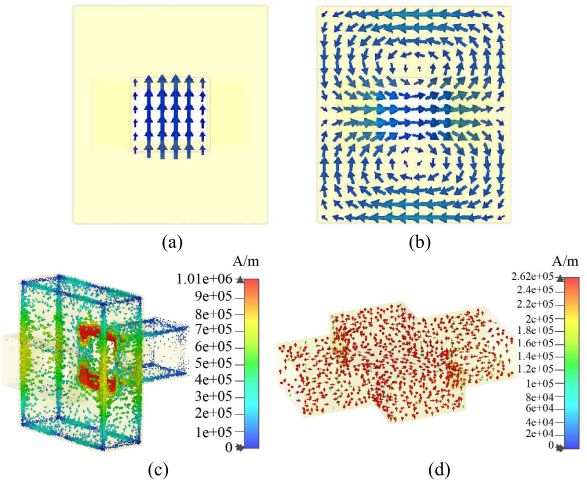

Fig. 3. (a) TE_{101} mode in cavity B. (b) TM_{120} mode in cavity A. (c) Surface current distribution on the stepped window. (d) Surface current distribution on the bandstop singlet in [13].

magnetic fields pass through the stepped window, they are simultaneously compressed in both directions. Thus, a parallel resonance circuit is equivalent to this SWR, as shown in Fig. 4(e) and (f). Therefore, when the condition of stored electric field energy equal to the stored magnetic field energy is satisfied, the stepped window can be regarded as a resonator [37].

Cavities A and B in Fig. 1(a) can be regarded as transmission lines in the equivalent circuit. Therefore, the characteristic impedances of the two transmission lines are matched when the stepped window resonates. According to [25] and [37], the characteristic impedances of TE and TM modes satisfy the following equations:

$$Z_{c\mathrm{TE}_{101}} = \frac{\eta}{\sqrt{1-\left(\frac{v}{2af_0}\right)^2}} \tag{1}$$

$$Z_{c\mathrm{TM}_{120}} = \eta\sqrt{1-\left(\frac{v}{2a'f_0}\right)^2-\left(\frac{v}{b'f_0}\right)^2} \tag{2}$$

where a, b, a', and b' are the dimensions marked in Fig. 4(e). η is the wave impedance of the cavity in the free space and λ is the wavelength. f_0 and v are the central frequency and propagation speed of electromagnetic waves in the free space. Since the impedance of TE_{101} mode and TM_{120} mode is matched, we get

$$Z_{c\mathrm{TE}_{101}} = Z_{c\mathrm{TM}_{120}}. \tag{3}$$

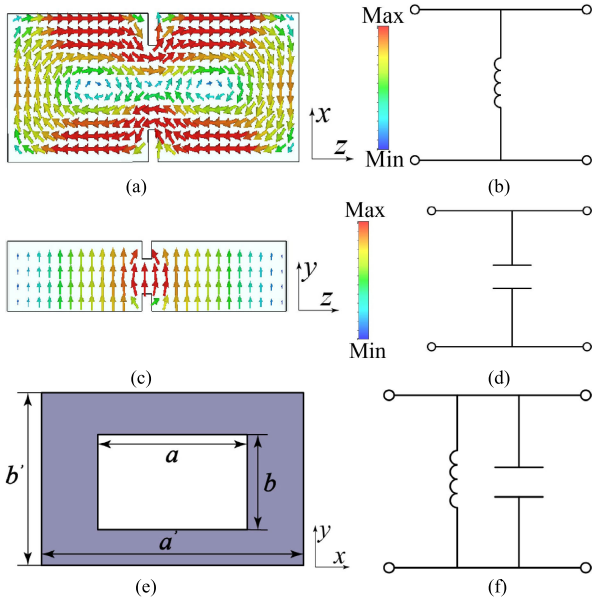

Fig. 4. (a) Symmetrical inductive diaphragm, (b), (d), and (f) equivalent circuit, (c) symmetrical capacitive diaphragm, and (e) rectangular resonant iris.

From (1) to (3), we solve the expression of central resonance frequency

$$f_0 = \frac{v}{2}\sqrt{\frac{b'^2+4a'^2}{a^2b'^2+4a^2a'^2+a'^2b'^2}}. \tag{4}$$

However, this formula is derived from impedance matching condition, which does not consider the parasitic effect caused by the discontinuity of the stepped window. A correction of (4) is needed, and we multiply a' by a correction factor p

$$f_0 = \frac{v}{2}\sqrt{\frac{b'^2+4(pa')^2}{a^2b'^2+4(pa^2a')^2+(pa')^2b'^2}}. \tag{5}$$

By changing the value of p and comparing the calculation results with the simulation results, we find that the two results are in good agreement when p is 1/3, which is shown in Fig. 5(a). Therefore, the final expression is as follows:

$$f_0 = \frac{v}{2}\sqrt{\frac{9b'^2+4a'^2}{9a^2b'^2+4a^2a'^2+a'^2b'^2}}. \tag{6}$$

For the verification of (6), some results are shown in Fig. 5(a), and variable m on the x-axis represents the multiplication factor by which all filter dimensions are scaled up or down. $f_{0\mathrm{sim}}$ and $f_{0\mathrm{cal}}$ are the central resonance frequencies of the proposed SWR that are simulated in CST and calculated by (6), respectively. It can be found that the simulation and calculation results are in good agreement, which shows that the derived (6) can accurately predict the resonator frequency within a wide frequency band ranging from 3 to 40 GHz. It is shown in Fig. 5(b) that changing the size ratio in the structure keeps the difference between $f_{0\mathrm{sim}}$ and $f_{0\mathrm{cal}}$ within a small range.

In order to explain the generation of the TZ and the factors which have an influence on the TZ and TP, an equivalent circuit model will be established. In general, the first step in modeling an equivalent circuit model is to design a low-pass

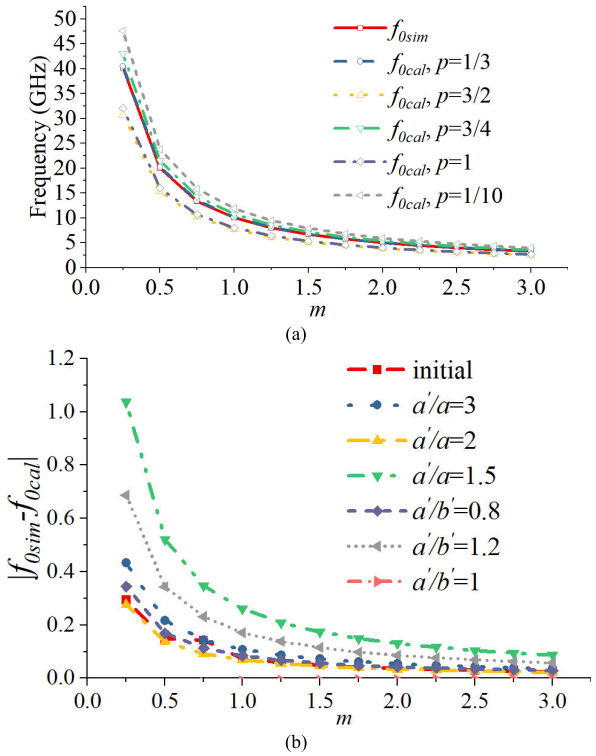

Fig. 5. (a) Resonant frequency comparison of SWR between EM simulated and calculated results in (5). (b) Effect of changing the size ratio in the structure on the difference between $f_{0\text{sim}}$ and $f_{0\text{cal}}$.

circuit model at normalized frequency. The frequency transformation formula (7) [36] can be used to convert the desired frequency to the normalized frequency

$$F = \frac{1}{\text{FBW}}\left(\frac{f}{f_c} - \frac{f_c}{f}\right) \tag{7}$$

where f_c is the central frequency, FBW is the fractional bandwidth of the BPF, and F is the normalized frequency. Each component also has a corresponding transformation process to complete the modeling of the equivalent circuit. Therefore, we can first design the model of the normalized frequency domain and then convert it to the desired frequency through the transformation formula.

The number of lumped capacitance and lumped inductance, which are frequency-dependent reactive elements, determines the order of the low-pass filter prototype network. In a ladder network, capacitance and inductance are interchanged by the dual-network theorem. Frequency-invariant reactance (FIR) elements can be used to design resonators, where FIR represents the offset between the resonant frequency of the resonator and the nominal frequency. Before modeling the entire circuit, there is some study about two kinds of basic resonators: bandpass resonator and bandstop resonator. Fig. 6 illustrates the low-pass prototype networks of the bandpass resonator and bandstop resonator, respectively. J_0 represents the J inverter, jB and jB_z are FIRs, which control offset of the resonant frequency, and C and L are the capacitance and inductance, respectively.

The process of establishing the equivalent circuit model starts from the transmission ($ABCD$) matrixes of each unit.

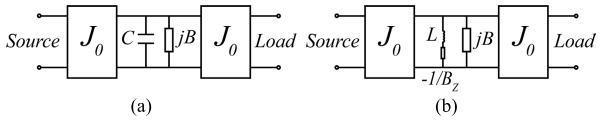

Fig. 6. Low-pass prototype networks. (a) Bandpass resonator. (b) Bandstop resonator.

The transmission ($ABCD$) matrixes of units are as follows:

$$[A_J] = \begin{bmatrix} 0 & j/J \\ jJ & 0 \end{bmatrix} \tag{8}$$

$$[A_C] = \begin{bmatrix} 1 & 0 \\ jfC & 1 \end{bmatrix} \tag{9}$$

$$[A_{jB}] = \begin{bmatrix} 1 & 0 \\ jB & 1 \end{bmatrix} \tag{10}$$

$$[A_{LB_Z}] = \begin{bmatrix} 1 & 0 \\ (jfL + jB_Z)^{-1} & 1 \end{bmatrix}. \tag{11}$$

From (8) to (11), we get the transmission ($ABCD$) matrixes of two basic resonators

$$[A_{\text{BPR}}] = [A_{J_0}][A_C][A_{jB}][A_{J_0}] \tag{12}$$

$$[A_{\text{BSR}}] = [A_{J_0}][A_{LB_Z}][A_{jB}][A_{J_0}]. \tag{13}$$

With reference to [37], we have the transformation formula for transmission ($ABCD$) matrix to S-parameters

$$S_{11} = \frac{A + B/Z_0 - CZ_0 - D}{A + B/Z_0 + CZ_0 + D} \tag{14}$$

$$S_{21} = \frac{2}{A + B/Z_0 + CZ_0 + D} \tag{15}$$

where Z_0 is the port impedance of the equivalent circuit. From (8) to (15), we solve S_{11} and S_{21}. Next, the numerators of S_{11} and S_{21} are extracted and solved, and the resulting roots are the frequency of the TP

$$f_{0\text{BPR}} = -B \tag{16}$$

$$f_{0\text{BSR}} = -B_z \tag{17}$$

where $f_{0\text{BPR}}$ and $f_{0\text{BSR}}$ are the resonance frequency of the bandpass and bandstop resonators, respectively. Fig. 7(a) and (b) shows the relationship between the values of the circuit components and the S-parameters of the entire circuit in Fig. 6(a) and (b), respectively.

It is illustrated in Fig. 7(a) that various normalized frequency responses can be obtained by setting different B values while $C = L = 1$. When the value of B is the same, the selectivity of the curve can be changed by adjusting the value of J. Moreover, the selectivity of the curve will reduce by increasing the value of J. In contrast, as shown in Fig. 7(b), the selectivity of the curve will increase when J increases, and the location of the bandstop resonance point is as described in formula (17).

The TZ could be analyzed by an equivalent circuit of the proposed SWR. Cavity A in Fig. 1(a) is a bandstop resonator in the proposed SWR, and the equivalent circuit model of the SWR is depicted in Fig. 8(a). Besides, Fig. 8(b) gives the comparison of $|S_{21}|$ between simulation results and synthesis response, where $J_{S1} = 0.08$, $J_{12} = 0.08$, $J_{2L} = 0.30$, $B_Z = 103.80$, $B_1 = 0$, $B_2 = -0.50$, and $L = C = 1.00$. It is obvious that the synthesis response and simulation results match well.

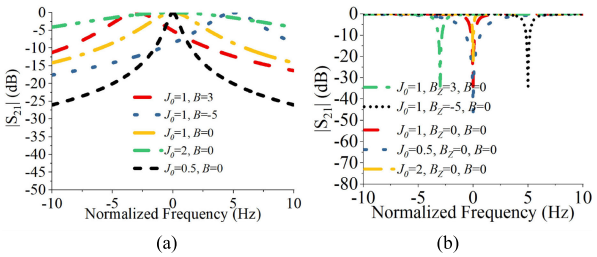

Fig. 7. Different S-parameters versus the changes of circuit component values. Normalized frequency response of (a) bandpass resonator and (b) band-stop resonator.

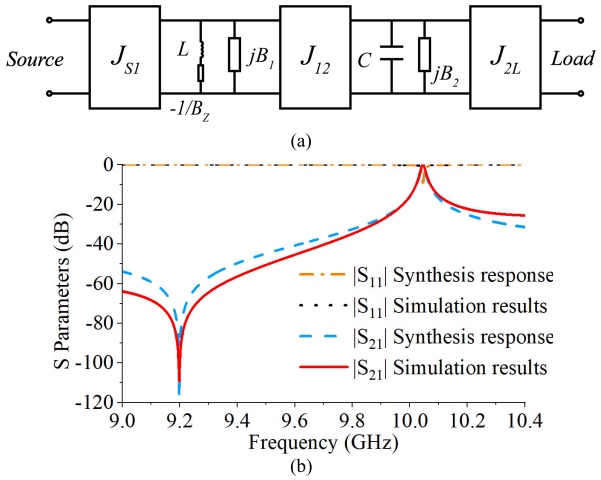

Fig. 8. (a) Equivalent circuit model of the SWR. (b) Comparison of $|S_{21}|$ between simulation response and synthesis response.

In the equivalent circuit, the position of the TPs and the TZ can be adjusted by changing the values of the FIR elements. Correspondingly, the sizes of the structure can control the resonance frequency and TZ. Moreover, Fig. 9(a) and (b) illustrates the relationships among central frequency, TZ, and the size of cavity A. It is obvious that the central resonance frequency and TZ are moving to the lower frequencies with the rises of a' and b'. This provides two good design parameters for fine-tuning the resonance frequency and TZ to the desired frequency. Meanwhile, the TZ and resonance frequency can also be adjusted by the size of cavity B. It is shown in Fig. 9(b) that the resonance frequency is moving to the lower frequencies with the increase of a. The position of the TZ is not affected by a but will move to the higher frequencies by increasing b. These physical parameters correspond to those of the equivalent circuit in Fig. 8(a).

III. Inline Stepped Window Cavity Filter With Two TZs

Based on the circuit analysis of the resonator above, a fourth-order inline stepped window cavity filter with three TZs is proposed, with its equivalent circuit and side view shown in Fig. 10. The four SWRs are marked in dotted lines. Cavities A', B', and C' control the coupling between the adjacent SWRs and generate TZs at the same time. Fig. 11(a) shows the 3-D view of the proposed cavity filter, which is a symmetrical structure consisting of four SWRs. Since the structure is symmetric along three axis of the structure, the dimensions of cavities A' and B' are the same. These two

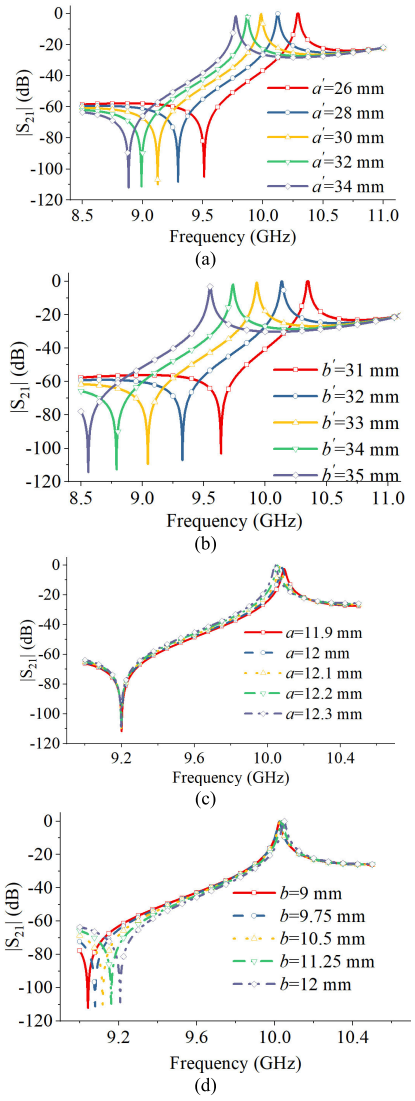

Fig. 9. Different resonant frequencies and TZs versus the changes of the sizes. (a) a'. (b) b'. (c) a. (d) b.

cavities correspond to B_{Z1} and B_{Z3} in Fig. 10, so there are two TZs at the same frequency. Fig. 11 illustrates the comparison of S-parameters between simulation results and synthesis response, which shows the well-matched between results. The parameters of optimized synthesis response are as follows: $J_{SZ1} = 0.3656$, $J_{Z11} = 0.3986$, $J_{12} = 0.9864$, $J_{2Z2} = 0.8340$, $J_{Z23} = 0.7659$, $J_{34} = 0.9565$, $J_{4Z3} = 0.6913$, $J_{Z3L} = 0.6779$, $B_{Z1} = 18.4$, $B_{Z2} = -1.79$, $B_{Z3} = 18.4$, $B_1 = -0.4483$, $B_2 = 0.4858$, $B_3 = 0.3461$, $B_4 = -0.1504$, $C_1 = 1$, $C_2 = 1$, $C_3 = 1$, $C_4 = 1$, $L_1 = 1$, $L_2 = 1$, $L_3 = 1$, $B_{01} = 0$, $B_{02} = 0$, and $B_{03} = 0$.

The external quality factors Q_e and coupling coefficient K between two resonators could be extracted through (18)–(20) [38] as follows:

$$Q_e = \frac{f_m}{\Delta f_{m\pm 90^\circ}} \tag{18}$$

$$K = \pm\frac{1}{2}\left(\frac{f_{02}}{f_{01}} + \frac{f_{01}}{f_{02}}\right)\sqrt{\left(\frac{f_{p2}^2 - f_{p1}^2}{f_{p2}^2 + f_{p1}^2}\right)^2 - \left(\frac{f_{02}^2 - f_{01}^2}{f_{02}^2 + f_{01}^2}\right)^2} \tag{19}$$

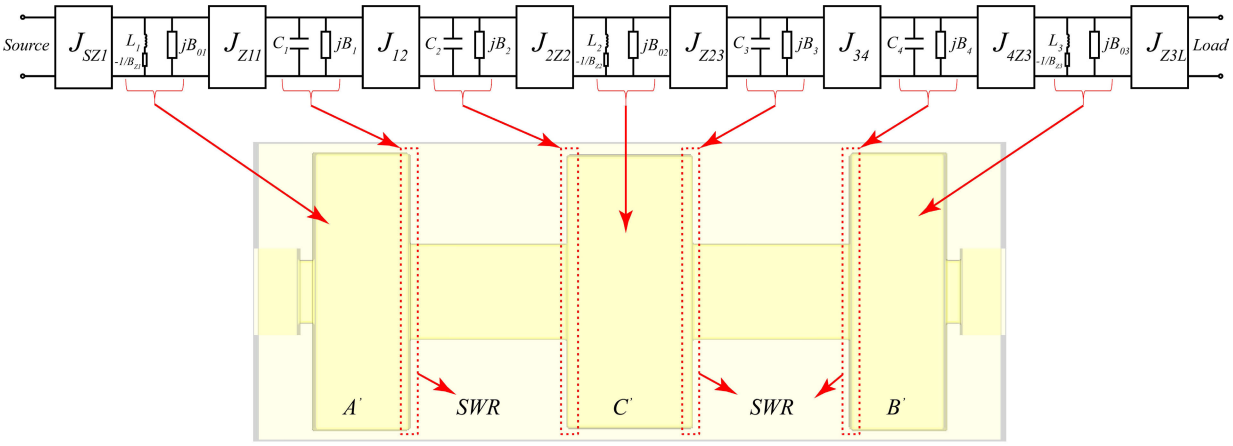

Fig. 10. Equivalent circuit model of the inline stepped window cavity filter.

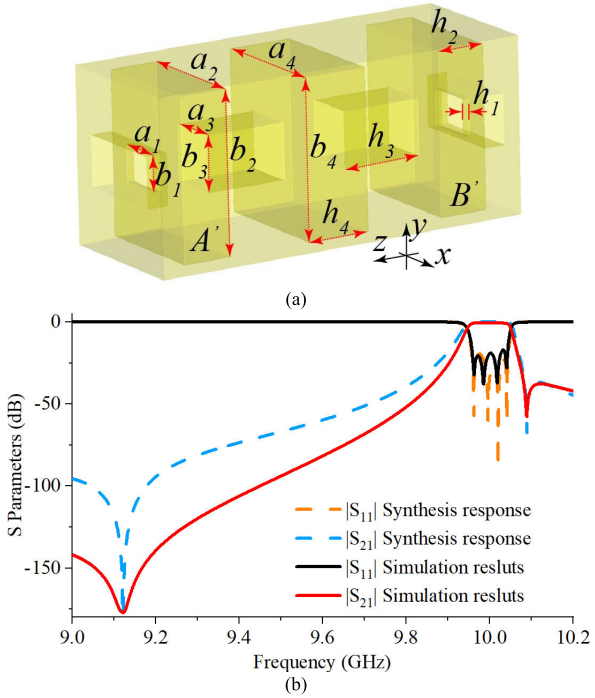

Fig. 11. (a) 3-D view of the proposed cavity filter. (b) Comparison of S-parameters between simulation results and synthesis response.

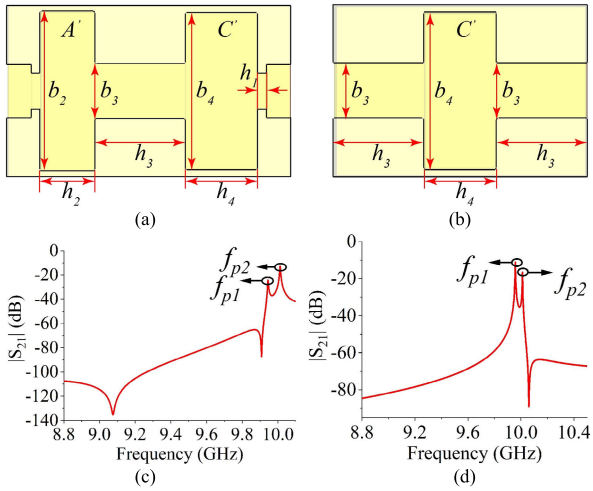

Fig. 12. (a) Side view of the extracting K_{12} structure. (b) Side view of the extracting K_{23} structure. (c) Simulation results for extracting K_{12}. (d) $|S_{21}|$ for extracting K_{23}.

$$K = \pm \frac{f_{p2}^2 - f_{p1}^2}{f_{p2}^2 + f_{p1}^2} \tag{20}$$

where f_m is the resonance frequency of the resonator, and $\Delta f_{m\pm 90^\circ}$ can be extracted from the absolute phase at f_m where a phase shift $\pm 90^\circ$. When the structures of the two coupled resonators are different, (19) can be used to extract coupling coefficient K, where f_{01} and f_{02} are the resonant frequencies of the two resonators, respectively. Besides, f_{p1} and f_{p2} are the respective resonant frequencies when two resonators are cascaded. Similarly, (20) can be used to extract coupling coefficient K when the structures of the two resonators are identical. In order to extract the TPs more accurately, a weak input coupling is adopted to show two resonance peaks clearly. Fig. 12(a) and (b) illustrates the structures for extracting coupling coefficients K_{12} and K_{23}, and Fig. 12(c) and (d) shows the simulation results of two structures, respectively. Since the dimensions of the two resonators are different, (19) is used to extract the coupling coefficient K_{12}. There are two TPs: f_{p1} and f_{p2}, and two TZs in Fig. 12(c). Obviously, this is consistent with the previous circuit analysis. Since the structure is symmetrical, the sizes of the two resonators are the same. Therefore, (20) can be used to extract K_{23}. There are two TPs and one TZ. Compared with Figs. 1(b) and 2(b), it can be seen that the proposed filter in this article is completely different from the singlet in [13].

Fig. 13 depicts the value of Q_e and coupling coefficient K as a function of various dimensions. Fig. 13(a)–(d) shows the variation of external quality factors with the sizes of the feeding coupling structure: a_1, b_1, h_1, and the dimensions of the first SWR: a_2, b_2, h_2, a_3, and b_3. The Q_e decreases with the rise of a_1 and b_1. In contrast, Q_e increases with the rise of a_2, a_3, b_3, h_1, and h_2. For b_2, Q_e will first shift down and then increase. It is illustrated in Fig. 13(b) that the size of the first and second SWRs can have an influence on K_{12} of the proposed BPF. As a_3 increases, K_{12} will first shift down and then rise dramatically, while when b_3 becomes larger, K_{12} will gently rise first and then fall. Finally, as h_3 increases, K_{12} will decrease sharply. Besides, it is shown in Fig. 13(c) and (d) that a_4, b_4, and h_4 can have various influences on K_{23}. K_{23} will decrease as a_4 increases. Moreover, K_{23} will first shift down

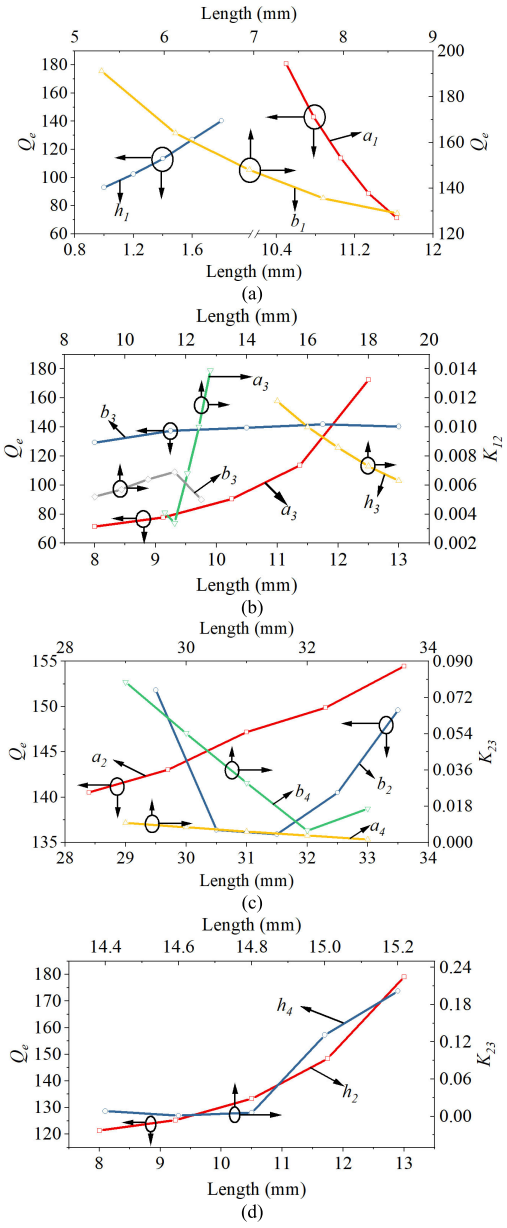

Fig. 13. (a) Relationships between Q_e and value of a_1, b_1, and h_1. (b) Effect to Q_e and K_{12} against with the changes of a_3, b_3, and h_3. (c) Values of Q_e and K_{23} against various a_2, b_2, a_4, and b_4. (d) Different Q_e and K_{23} against with the changes of h_2 and h_4.

and then increase with the rise of b_4, and K_{23} will decrease and then increase with the rise of h_4.

IV. Experimental Results

A fourth-order stepped window BPF is proposed and fabricated using brass. Fig. 14(a) and (b) shows the photographs of the external view and internal view of the fabricated filter, respectively. The physical size parameters are as follows: $a_1 = 10.80$, $b_1 = 7.38$, $h_1 = 1.81$, $a_2 = 29.12$, $b_2 = 32.56$, $h_2 = 11.23$, $a_3 = 12.04$, $b_3 = 11.21$, $h_3 = 18.56$, $a_4 = 31.04$, $b_4 = 32.02$, and $h_4 = 14.79$ (all in mm). The simulated and measured results are illustrated in Fig. 15(a) with wideband frequency response. It is shown that two results match well, the measured center frequency is at 10 GHz, and the measured 3-dB fractional bandwidth of the filter is from

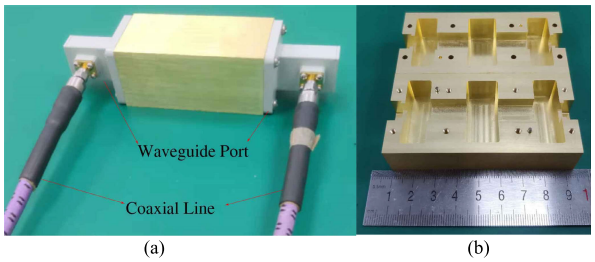

Fig. 14. Photograph of the fabricated stepped window BPF. (a) External view. (b) Inside view.

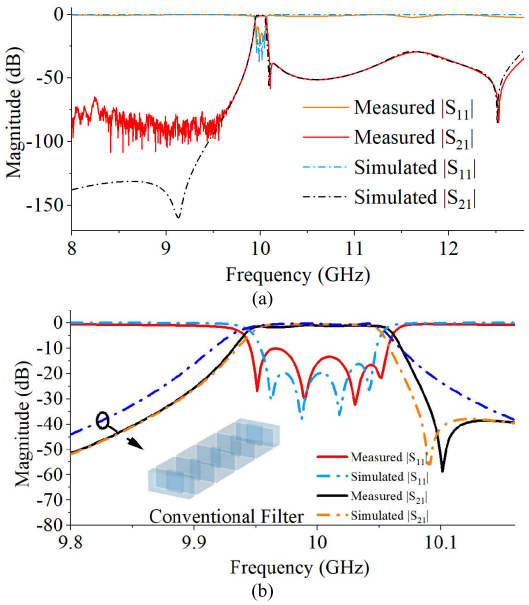

Fig. 15. Comparison of simulated and measured S-parameter frequency responses. (a) Wideband frequency response. (b) Narrowband frequency response with conventional cavity filter comparison.

9.94 to 10.06 GHz (1%). The measured return loss of the filter is below 10 dB within the passband and the IL is around 0.9 dB in the passband. The IL is around 0.5 dB in simulation, and the discrepancy between simulation and measurement may be caused by the roughness and gaps between metal parts, which is not considered in simulation. It is noteworthy that the proposed SWR filter compares with the conventional inline cavity resonator filter with filter same specifications, as shown in Fig. 15(b). The selectivity is much better at roll-off region in higher frequency.

From 10.08 to 12.97 GHz, there is a good upper stopband rejection and has more than 20 dB. Two standard coaxial-to-waveguide transitions (WR-90) are used as input–output waveguide feeding ports for measurement. Therefore, the differences between simulation results and measurement results are mainly caused by fabrication and the losses from the parasitic ohmic loss between the installation gap of each metal structure. Two TZs are produced by three shunt loading cavities, one TZ is located at 10.1 GHz, and the other TZ is below the noise floor of the vector network analyzer. It can be viewed from the narrowband frequency response in Fig. 15(b) that the selectivity of the proposed stepped window BPF is better than that of the conventional cavity resonator BPF using iris coupling structure. Moreover, Table I illustrates the comparison between this work and the state-of-the-art cavity

TABLE I
COMPARISONS WITH PREVIOUSLY REPORTED CAVITY BPFS

Ref.	Resonator	f_0 (GHz)	FBW (%)	IL (dB)	Q_u	TP	TZ	Manufacturing techniques	Size (λ_c is the wavelength of the center frequency)
[14]	rectangular cavity	19.82 GHz	1.21 %	N/A	N/A	6	2	N/A	2.14*0.56*7.38 λ_c^3
[27]	Iris resonator	14.25 GHz	4.56 %	N/A	N/A	7	0	N/A	0.75*0.38*3.01 λ_c^3
[32]	Iris resonator and rectangular cavity resonator	9.08 GHz	9.50 %	0.15 dB	N/A	3	1	3-D printing	1.64*1.00*0.61 λ_c^3
[35] Filter I	Iris resonator and rectangular cavity resonator	7.50 GHz and 10.00GHz	13.33 % and 5.00 %	0.17 dB	1415	5 and 4	2 and 2	CNC	0.57*1.78*2.96 λ_c^3
[35] Filter II	Iris resonator and rectangular cavity resonator	7.55 GHz	17.54 %	0.19 dB	1986	9	3	CNC	0.58*1.95*3.80 λ_c^3
This work	Stepped window resonator	10.00 GHz	1.00 %	0.90 dB	3883	4	2	CNC	2.67*1.03*1.09 λ_c^3

N/A: Not available; CNC: Computer Numerical Control; FBW: Fractional Bandwidth

BPFs. As can be seen from Table I, the size of the proposed filter is much smaller than the reported filter, which only uses rectangular waveguide resonators. Finally, Q_u and the first spurious passband also have good performance.

V. CONCLUSION

An inline stepped window BPF with two TZs is proposed in this article. The structure of this BPF is very simple and easy to fabricate. It is noted that the volume of the proposed filter is much smaller than the cavity filter using cavity resonators. Compared with the reported iris BPFs, Q_u of the proposed filter is large, which is a very good candidate to design narrowband BPF. Moreover, the equivalent circuit is created to explain the working mechanism of the proposed filter. The synthesis frequency response, simulation results, and fabricated measurement match well to experimentally verify the synthesis theory and the proposed SWR filter. Finally, the proposed BPF is useful in the X-band for the radar communication system application because of its easy fabrication, low cost, and simple design.

REFERENCES

[1] N. Thomson and J.-S. Hong, "Compact ultra-wideband microstrip/coplanar waveguide bandpass filter," *IEEE Microw. Wireless Compon. Lett.*, vol. 17, no. 3, pp. 184–186, Mar. 2007.

[2] H. Shaman and J.-S. Hong, "A novel ultra-wideband (UWB) bandpass filter (BPF) with pairs of transmission zeroes," *IEEE Microw. Wireless Compon. Lett.*, vol. 17, no. 2, pp. 121–123, Feb. 2007.

[3] Z.-C. Zhang, S.-W. Wong, X. Yu, B. Zhao, D. Wang, and R. Chen, "Compact quadruple-mode wideband bandpass filter using L-shaped feed-line in a single cavity," *IEEE Microw. Wireless Compon. Lett.*, vol. 31, no. 10, pp. 1111–1114, Oct. 2021.

[4] Z.-C. Zhang et al., "Miniaturization of triple-mode wideband bandpass filters," *IEEE Trans. Compon., Packag., Manuf. Technol.*, vol. 12, no. 8, pp. 1368–1374, Aug. 2022, doi: 10.1109/TCPMT.2022.3195729.

[5] Z.-C. Guo, S.-W. Wong, and L. Zhu, "Triple-passband cavity filters with high selectivity under operation of triple modes," *IEEE Trans. Compon., Packag., Manuf. Technol.*, vol. 9, no. 7, pp. 1337–1344, Jul. 2019.

[6] S. W. Wong, K. Wang, Z.-N. Chen, and Q.-X. Chu, "Electric coupling structure of substrate integrated waveguide (SIW) for the application of 140-GHz bandpass filter on LTCC," *IEEE Trans. Compon., Packag., Manuf. Technol.*, vol. 4, no. 2, pp. 316–322, Feb. 2014.

[7] S.-W. Wong, R. S. Chen, K. Wang, Z.-N. Chen, and Q.-X. Chu, "U-shape slots structure on substrate integrated waveguide for 40-GHz bandpass filter using LTCC technology," *IEEE Trans. Compon., Packag., Manuf. Technol.*, vol. 5, no. 1, pp. 128–134, Jan. 2015.

[8] S.-W. Wong, F. Deng, J.-Y. Lin, Y.-M. Wu, L. Zhu, and Q.-X. Chu, "An independently four-channel cavity diplexer with 1.1–2.8 GHz tunable range," *IEEE Microw. Wireless Compon. Lett.*, vol. 27, no. 8, pp. 709–711, Aug. 2017.

[9] S.-W. Wong, R.-S. Chen, J.-Y. Lin, L. Zhu, and Q.-X. Chu, "Substrate integrated waveguide quasi-elliptic filter using slot-coupled and microstrip-line cross-coupled structures," *IEEE Trans. Compon., Packag., Manuf. Technol.*, vol. 6, no. 12, pp. 1881–1888, Dec. 2016.

[10] M. Latif, G. Macchiarella, and F. Mukhtar, "A novel coupling structure for inline realization of cross-coupled rectangular waveguide filters," *IEEE Access*, vol. 8, pp. 107527–107538, 2020.

[11] S. Bastioli, "Nonresonating mode waveguide filters," *IEEE Microw. Mag.*, vol. 12, no. 6, pp. 77–86, Oct. 2011.

[12] G. Macchiarella, G. G. Gentili, C. Tomassoni, S. Bastioli, and R. V. Snyder, "Design of waveguide filters with cascaded singlets through a synthesis-based approach," *IEEE Trans. Microw. Theory Techn.*, vol. 68, no. 6, pp. 2308–2319, Jun. 2020.

[13] G. Macchiarella, G. Gentili, and L. Accatino, "Stopband singlet: A novel structure implementing resonating couplings," *IEEE Microw. Wireless Compon. Lett.*, vol. 30, no. 5, pp. 473–476, May 2020.

[14] G. Macchiarella, G. G. Gentili, N. Delmonte, L. Silvestri, and M. Bozzi, "Design of inline waveguide filters with frequency-variant couplings producing transmission zeros," *IEEE Trans. Microw. Theory Techn.*, vol. 69, no. 8, pp. 3746–3758, Aug. 2021.

[15] R.-S. Chen et al., "Reconfigurable cavity bandpass filters using fluid dielectric," *IEEE Trans. Ind. Electron.*, vol. 68, no. 9, pp. 8603–8614, Sep. 2021.

[16] Z.-C. Guo et al., "Triple-mode cavity bandpass filter on doublet with controllable transmission zeros," *IEEE Access*, vol. 5, pp. 6969–6977, 2017.

[17] J.-Y. Lin, S.-W. Wong, L. Zhu, and Q.-X. Chu, "Design of miniaturized triplexers via sharing a single triple-mode cavity resonator," *IEEE Trans. Microw. Theory Techn.*, vol. 65, no. 10, pp. 3877–3884, Oct. 2017.

[18] Y. Xie, F.-C. Chen, and Q.-X. Chu, "Tunable cavity filter and diplexer using in-line dual-post resonators," *IEEE Trans. Microw. Theory Techn.*, vol. 70, no. 6, pp. 3188–3199, Jun. 2022.

[19] Y. Wang and M. Yu, "True inline cross-coupled coaxial cavity filters," *IEEE Trans. Microw. Theory Techn.*, vol. 57, no. 12, pp. 2958–2965, Dec. 2009.

[20] H. Wang and Q.-X. Chu, "An inline coaxial quasi-elliptic filter with controllable mixed electric and magnetic coupling," *IEEE Trans. Microw. Theory Techn.*, vol. 57, no. 3, pp. 667–673, Mar. 2009.
[21] H. Hu and K.-L. Wu, "A deterministic EM design technique for general waveguide dual-mode bandpass filters," *IEEE Trans. Microw. Theory Techn.*, vol. 61, no. 2, pp. 800–807, Feb. 2013.
[22] Z.-C. Zhang et al., "Triple-mode dielectric-loaded cylindrical cavity diplexer using novel packaging technique for LTE base-station applications," *IEEE Trans. Compon., Packag., Manuf. Technol.*, vol. 6, no. 3, pp. 383–389, Mar. 2016.
[23] Y.-M. Wu, S.-W. Wong, H. Wong, and F.-C. Chen, "A design of bandwidth-enhanced cavity-backed slot filtenna using resonance windows," *IEEE Trans. Antennas Propag.*, vol. 67, no. 3, pp. 1926–1930, Mar. 2019.
[24] J.-Y. Lin, S.-W. Wong, Y.-M. Wu, Y. Yang, L. Zhu, and Y. He, "Three-way multiple-mode cavity filtering crossover for narrowband and broadband applications," *IEEE Trans. Microw. Theory Techn.*, vol. 67, no. 3, pp. 896–905, Mar. 2019.
[25] T.-S. Chen, "Characteristics of waveguide resonant-iris filters (Correspondence)," *IEEE Trans. Microw. Theory Techn.*, vol. MTT-15, no. 4, pp. 260–262, Apr. 1967.
[26] R.-M. Barrio-Garrido, S. Llorente-Romano, A. Garcia-Lamperez, and M. Salazar-Palma, "Design of broadband directly coupled non-centred resonant irises filters," in *Proc. 33rd Eur. Microw. Conf.*, Oct. 2003, pp. 219–222.
[27] C. Zong-Tao and L. Sheng-Xian, "Design of microwave filter with resonant irises of resonant windows at different location," in *Proc. IEEE Int. Conf. Microw. Technol. Comput. Electromagn.*, May 2011, pp. 156–159.
[28] M. Piloni, R. Ravenelli, and M. Guglielmi, "Resonant aperture filters in rectangular waveguide," in *IEEE MTT-S Int. Microw. Symp. Dig.*, Jun. 1999, pp. 911–914.
[29] M. Capurso, M. Piloni, and M. Guglielmi, "Resonant aperture filters: Improved out-of-band rejection and size reduction," in *Proc. 31st Eur. Microw. Conf.*, Sep. 2001, pp. 1–4.
[30] U. Rosenberg, S. Amari, J. Bornemann, and R. Vahldieck, "Compact pseudo-highpass filters formed by cavity and iris resonators," in *Proc. 34th Eur. Microw. Conf.*, vol. 2, Oct. 2004, pp. 985–988.
[31] U. Rosenberg, S. Amari, and J. Bornemann, "Mixed-resonance compact in-line pseudo-elliptic filters," in *IEEE MTT-S Int. Microw. Symp. Dig.*, vol. 1, Jun. 2003, pp. 479–482.
[32] L. Qian, R. Martinez, M. Salek, M. Attallah, Y. Wang, and M. J. Lancaster, "Compact monolithic SLM 3D-printed filters using pole-generating resonant irises," in *Proc. 51st Eur. Microw. Conf. (EuMC)*, Apr. 2022, pp. 118–121.
[33] J. Rao, K. Nai, J. Marques-Hueso, P. Vaitukaitis, and J. Hong, "Inline quasi-elliptic bandpass filter based on metal 3-D printing technology," *IEEE Trans. Microw. Theory Techn.*, vol. 70, no. 4, pp. 2156–2164, Apr. 2022.
[34] J. F. V. Sullca, S. Cogollos, M. Guglielmi, and V. E. Boria, "Dual-band filters in rectangular waveguide based on resonant apertures," in *IEEE MTT-S Int. Microw. Symp. Dig.*, Jun. 2021, pp. 192–195.
[35] J. F. V. Sullca, S. Cogollos, V. E. Boria, and M. Guglielmi, "Compact dual-band and wideband filters with resonant apertures in rectangular waveguide," *IEEE Trans. Microw. Theory Techn.*, vol. 70, no. 6, pp. 3125–3140, Jun. 2022.
[36] R. J. Cameron, C. M. Kudsia, and R. R. Mansour, *Microwave Filters for Communication Systems: Fundamentals, Design, and Applications*. New York, NY, USA: Wiley, 2007.
[37] D. M. Pozar, *Microwave Engineering*. Hoboken, NJ, USA: Wiley, 2011.
[38] J.-S. Hong and M. J. Lancaster, *Microstrip Filters for RF/Microwave Applications*. New York, NY, USA: Wiley, 2001.

Xuzhou Yu (Student Member, IEEE) received the B.E. degree from the School of Electronic and Information Engineering, Tianjin University (TJU), Tianjin, China, in 2019, and the M.E. degree from the College of Electronics and Information Engineering, Shenzhen University (SZU), Shenzhen, China, in 2023.

His current research interests include microwave cavity circuit design.

Sai-Wai Wong (Senior Member, IEEE) received the B.S. degree in electronic engineering from the Hong Kong University of Science and Technology, Hong Kong, in 2003, and the M.Sc. and Ph.D. degrees in communication engineering from Nanyang Technological University, Singapore, in 2006 and 2009, respectively.

From July 2003 to July 2005, he was with the Lead Engineering Department in mainland of China with two Hong Kong manufacturing companies. From 2009 to 2010, he was a Research Fellow with the Institute for Infocomm Research, Singapore. Since 2010, he has been an Associate Professor and became a Full Professor with the School of Electronic and Information Engineering, South China University of Technology, Guangzhou, China. In 2016, he was a Visiting Professor with the City University of Hong Kong, Hong Kong. In 2017, he was a Visiting Professor with the University of Macau, Macau, China. Since 2017, he has been a Full Professor at the College of Electronics and Information Engineering, Shenzhen University, Shenzhen, China. His current research interests include RF/microwave circuit and antenna design.

Dr. Wong was a recipient of the New Century Excellent Talents in University (NCET) Award in 2013 and the Shenzhen Overseas High-Caliber Personnel Level C in 2018. He is a reviewer for several top-tier journals.

Jing-Yu Lin (Member, IEEE) received the B.E. degree from Southwest Jiaotong University (SWJTU), Chengdu, China, in 2016, the M.E. degree from the School of Electronic and Information Engineering, South China University of Technology (SCUT), Guangzhou, China, in 2018, and the Ph.D. degree from the University of Technology Sydney (UTS), Ultimo, NSW, Australia, in 2022.

From October 2017 to February 2019, he was as an Exchange Student at UTS. He is currently an Associate Professor with the Institute of Electromagnetics and Acoustics, Xiamen University, Xiamen, China. His current research interests include microwave, millimeter-wave, and terahertz waveguide circuit and antenna designs.

Dr. Lin was a recipient of the IEEE MTT-S Graduate Student Fellowship Awards in 2020 and the Xiamen University Nanqiang Talent Plan Class B in 2022.

Yejun He (Senior Member, IEEE) received the Ph.D. degree in information and communication engineering from the Huazhong University of Science and Technology, Wuhan, China, in 2005.

From 2005 to 2006, he was a Research Associate with the Department of Electronic and Information Engineering, Hong Kong Polytechnic University, Hong Kong. From 2006 to 2007, he was a Research Associate with the Department of Electronic Engineering, Faculty of Engineering, The Chinese University of Hong Kong, Hong Kong. In 2012, he was a Visiting Professor with the Department of Electrical and Computer Engineering, University of Waterloo, Waterloo, ON, Canada. From 2013 to 2015, he was an Advanced Visiting Scholar (Visiting Professor) with the School of Electrical and Computer Engineering, Georgia Institute of Technology, Atlanta, GA, USA. Since 2011, he has been a Full Professor with the College of Electronics and Information Engineering, Shenzhen University, Shenzhen, China, where he is the Director of Guangdong Engineering Research Center of Base Station Antennas and Propagation and the Director of Shenzhen Key Laboratory of Antennas and Propagation, Shenzhen. He was selected as the Pengcheng Scholar Distinguished Professor, Shenzhen, and the Minjiang Scholar Chair Professor of Fujian Province. He has authored or coauthored more than 250 research papers, books (chapters), and holds about 20 patents. His research interests include wireless communications, antennas, and radio frequency.

Dr. He is a fellow of IET, a Senior Member of the China Institute of Communications, and a Senior Member of the China Institute of Electronics. He was a recipient of the Shenzhen Overseas High-Caliber Personnel Level B ("Peacock Plan Award" B) and Shenzhen High-Level Professional Talent (Local Leading Talent). He was a recipient of the Shenzhen Science and Technology Progress Award and the Guangdong Provincial Science and Technology Progress Award in 2017 and 2018, respectively. He is currently the Chair of IEEE Antennas and Propagation Society-Shenzhen Chapter and obtained 2022 IEEE APS Outstanding Chapter Award. He was a reviewer for various top-tier journals. He was also the technical program committee member or the session chair of various conferences. He was an Associate Editor for *Security and Commu-nication Networks Journal* and IEEE NETWORK. He is an Associate Editor for the IEEE TRANSACTIONS ON ANTENNAS AND PROPAGATION, IEEE TRANSACTIONS ON MOBILE COMPUTING, *IEEE Antennas and Propaga-tion Magazine*, IEEE ANTENNAS AND WIRELESS PROPAGATION LETTERS, *International Journal of Communication Systems*, *China Communications*, and *Wireless Communications and Mobile Computing*.

Wenting Li (Member, IEEE) received the B.S. degree in electronic information engineering and the M.S. degree in electromagnetic field and microwave technology from Northwestern Polytechnical University, Xi'an, China, in 2011 and 2014, respectively, and the Ph.D. degree in electronic engineering from the University of Kent, Canterbury, U.K., in 2019.

He is currently an Assistant Professor with the College of Electronics and Information Engineering, Shenzhen University, Shenzhen, China. His current research interests include reflectarray antennas, reconfigurable antennas, circularly polarized antennas, and multibeam antennas.

Dr. Li was a recipient of the Shenzhen Overseas High-Caliber Personnel Level C ("Peacock Plan Award" C).

Long Zhang (Member, IEEE) received the B.S. and M.S. degrees in electrical engineering from the Huazhong University of Science and Technology (HUST), Wuhan, China, in 2009 and 2012, respectively, and the Ph.D. degree in electronic engineering from the University of Kent, Canterbury, U.K, in 2017.

From January 2018 to April 2018, he was a Research Fellow with the Poly-Grames Research Center, Polytechnique Montreal, Montreal, QC, Canada. He is currently an Assistant Professor with the College of Electronics and Information Engineering, Shenzhen University, Shenzhen, China. His current research interests include millimeter-wave antennas and arrays, tightly coupled arrays, reflectarrays and transmitarrays, characteristic mode theory, and machine learning methods for antenna and metasurface design.

Dr. Zhang has served as a TPC member and the session chair for several international conferences. He served as the Lead Guest Editor of *Electronics Letters* for a Special Issue on "Wideband/Multiband Millimeter-Wave Antennas for 5G/6G and Radar Applications" in 2023. He also serves as a reviewer for more than ten journals, including the IEEE TRANSACTIONS ON ANTENNAS AND PROPAGATION, IEEE TRANSACTIONS ON MICROWAVE THEORY AND TECHNIQUES, IEEE TRANSACTIONS ON CIRCUITS AND SYSTEMS II: EXPRESS BRIEFS, IEEE TRANSACTIONS ON VEHICULAR TECHNOLOGY, and the IEEE ANTENNAS AND WIRELESS PROPAGATION LETTERS.

Lei Zhu (Fellow, IEEE) received the B.Eng. and M.Eng. degrees in radio engineering from the Nanjing Institute of Technology (now Southeast University), Nanjing, China, in 1985 and 1988, respectively, and the Ph.D. degree in electronic engineering from the University of Electro-Communications, Tokyo, Japan, in 1993.

From 1993 to 1996, he was a Research Engineer with Matsushita-Kotobuki Electronics Industries Ltd., Tokyo, Japan. From 1996 to 2000, he was a Research Fellow with the École Polytechnique de Montreal, Montreal, QC, Canada. From 2000 to 2013, he was an Associate Professor with the School of Electrical and Electronic Engineering, Nanyang Technological University, Singapore. He joined the Faculty of Science and Technology, University of Macau, Macau, China, as a Full Professor in August 2013, and has been a Distinguished Professor since December 2016. Since September 2014, he has been serving as the Head of Department of Electrical and Computer Engineering, University of Macau. So far, he has authored or coauthored more than 350 papers in international journals and conference proceedings. His papers have been cited more than 4160 times with the H-index of 36 (source: ISI Web of Science). His research interests include microwave circuits, guided-wave periodic structures, antennas, and computational electromagnetic techniques.

Dr. Zhu served as a member of IEEE MTT-S Fellow Evaluation Committee from 2013 to 2015, and has been serving as a member of IEEE AP-S Fellows Committee, since 2015. He was a recipient of the 1997 Asia–Pacific Microwave Prize Award, the 1996 Silver Award of Excellent Invention from Matsushita-Kotobuki Electronics Industries Ltd., and the 1993 First-Order Achievement Award in Science and Technology from the National Education Committee, China. He was the Associate Editor for the IEEE TRANSACTIONS ON MICROWAVE THEORY AND TECHNIQUES from 2010 to 2013 and IEEE MICROWAVE AND WIRELESS COMPONENTS LETTERS from 2006 to 2012. He served as the General Chair of the 2008 IEEE MTT-S International Microwave Workshop Series on the Art of Miniaturizing RF and Microwave Passive Components, Chengdu, China, and the Technical Program Committee Co-Chair of the 2009 Asia–Pacific Microwave Conference, Singapore.

Li Yu received the B.S. degree from the School of Materials Science and Engineering, Tianjin University, Tianjin, China, in 1999, and the Ph.D. degree in computer science from the School of Computer Science and Technology, Tianjin University, in 2009.

From 2009 to 2012, he was a Microwave Engineer (Senior) with the 38th Research Institute of China Electronics Technology Group Corporation. Since 2012, he has been an Assistant Professor with Tianjin Medical University, Tianjin. His research interests include bioelectromagnetics, computer simulation, and bioinformatics algorithm.